© 2020. Published by The Company of Biologists Ltd | Development (2020) 147, dev190983. doi:10.1242/dev.190983

RESEARCH REPORT

Localised Collagen2a1 secretion supports lymphatic endothelial cell migration in the zebrafish embryo

Smrita Chaudhury[1], Kazuhide S. Okuda[1,2], Katarzyna Koltowska[1,*], Anne K. Lagendijk[1], Scott Paterson[1,2], Gregory J. Baillie[1], Cas Simons[1,‡], Kelly A. Smith[1,3], Benjamin M. Hogan[1,2,4,§] and Neil I. Bower[1,§]

ABSTRACT

The lymphatic vasculature develops primarily from pre-existing veins. A pool of lymphatic endothelial cells (LECs) first sprouts from cardinal veins followed by migration and proliferation to colonise embryonic tissues. Although much is known about the molecular regulation of LEC fate and sprouting during early lymphangiogenesis, we know far less about the instructive and permissive signals that support LEC migration through the embryo. Using a forward genetic screen, we identified *mbtps1* and *sec23a*, components of the COP-II protein secretory pathway, as essential for developmental lymphangiogenesis. In both mutants, LECs initially depart the cardinal vein but then fail in their ongoing migration. A key cargo that failed to be secreted in both mutants was a type II collagen (Col2a1). Col2a1 is normally secreted by notochord sheath cells, alongside which LECs migrate. *col2a1a* mutants displayed defects in the migratory behaviour of LECs and failed lymphangiogenesis. These studies thus identify Col2a1 as a key cargo secreted by notochord sheath cells and required for the migration of LECs. These findings combine with our current understanding to suggest that successive cell-to-cell and cell-matrix interactions regulate the migration of LECs through the embryonic environment during development.

KEY WORDS: *Sec23a*, *Mbtps1*, *Col2a1*, Lymphangiogenesis, Extracellular matrix, Collagen, Zebrafish

INTRODUCTION

The lymphatic vasculature drains tissue fluid and fatty acids, regulates immune cell trafficking and is important in a range of pathologies that include cancer and cardiovascular disease (Ma et al., 2018; Petrova and Koh, 2018). The development of new lymphatic vessels occurs primarily from pre-existing veins and is controlled by mechanisms that are conserved between zebrafish and mammals (Hogan and Schulte-Merker, 2017). In the zebrafish trunk, secondary sprouting occurs from the posterior cardinal vein (PCV) from 32 h post fertilisation (hpf) and produces the first lymphatic endothelial cell (LEC) progenitors (parachordal LECs; PLs) as well as the intersegmental veins (vISVs). In this dorsal angiogenic sprouting event, half the secondary sprouts will form vISVs by anastomosing with adjacent arteries, whereas the remaining half migrate dorsally to the horizontal myoseptum (HM) to form PLs (Bussmann et al., 2010). The PLs proliferate, leave the HM and migrate dorsally and ventrally to form the major lymphatic vessels of the trunk: the thoracic duct (TD), dorsal longitudinal lymphatic vessel (DLLV), and intersegmental lymphatic vessels (ISLVs) (Hogan et al., 2009; Yaniv et al., 2006). LECs migrate progressively between different locations in the embryo, involving serial contact with different cell types and substrates along the way. We are beginning to understand some of the cellular interactions and molecular guidance cues involved along the LEC migration route. For example, chemokine signalling from arteries and local secretion of Vegfc-processing machinery from fibroblasts and neurons are essential non-autonomously acting signals driving lymphangiogenesis (Cha et al., 2012; Lim et al., 2011; Wang et al., 2020). Yet, the identity of all of the key constituents of the LEC microenvironment and how they act in sequence to control LEC migration remains to be fully appreciated.

The development of LECs is intimately associated with and requires the extracellular matrix (ECM) (Frye et al., 2018; Planas-Paz et al., 2012). The ECM is composed of many structural proteins required for cell migration and adhesion, such as collagens, Fibronectin, integrins and Hyaluronan, and also acts as an environment for normal processing and presentation of growth factors such as Vegfc (Jeltsch et al., 2014; Joukov et al., 1997; Le Guen et al., 2014). *In vitro* studies have demonstrated that Collagen 1 facilitates LEC and blood endothelial cell (BEC) capillary formation and migration, involving collagen ligation to the collagen binding integrins α1β1 and α2β1 with α2β1(Davis and Camarillo, 1996; Podgrabinska et al., 2002; Seo et al., 2014; Whelan and Senger, 2003). *In vivo*, several ECM components and regulators can influence the development, maturation and function of lymphatics, including Reelin, Itga9, Emilin1, Hyaluronan and Polydom (Bazigou et al., 2009; Danussi et al., 2008; De Angelis et al., 2017; Karpanen et al., 2017; Lutter et al., 2012; Morooka et al., 2017). How different matrix factors pattern the early steps in lymphatic development and the *in vivo* roles of the many members of large families of structural proteins, such as the collagens, remains to be fully understood.

In this study, we used a forward genetic screen to identify new regulators of lymphatic vessel development. We found that s*ec23a* and *mbtps1* mutants exhibit defects in the migration of PLs from the HM to form a functional trunk lymphatic vasculature. Both mutants display a failure of Collagen2a1 (Col2a1) secretion by notochord sheath cells (NSCs). PLs migrate immediately along the NSCs following their departure from the PCV. Analysis of *col2a1a*

[1]Division of Genomics of Development and Disease, Institute for Molecular Bioscience, The University of Queensland, St Lucia, QLD 4072, Australia. [2]Peter MacCallum Cancer Centre, Organogenesis and Cancer Program, Melbourne, Victoria 3000, Australia. [3]Department of Physiology, University of Melbourne, Parkville, Victoria 3010, Australia. [4]Department of Anatomy and Neuroscience, University of Melbourne, Parkville, Victoria 3010, Australia.
*Present address: Department of Immunology, Genetics and Pathology, Uppsala University, Dag Hammarskjölds väg 20, 751 85, Uppsala, Sweden. ‡Present address: Murdoch Children's Research Institute, Royal Children's Hospital, Flemington Road, Parkville, Victoria, 3052, Australia.

§Authors for correspondence (ben.hogan@petermac.org; n.bower@imb.uq.edu.au)

C.S., 0000-0003-3147-8042; B.M.H., 0000-0002-0651-7065; N.I.B., 0000-0002-6764-6063

Handling Editor: Steve Wilson
Received 27 March 2020; Accepted 7 August 2020

Development (2020) 147, dev190983. doi:10.1242/dev.190983

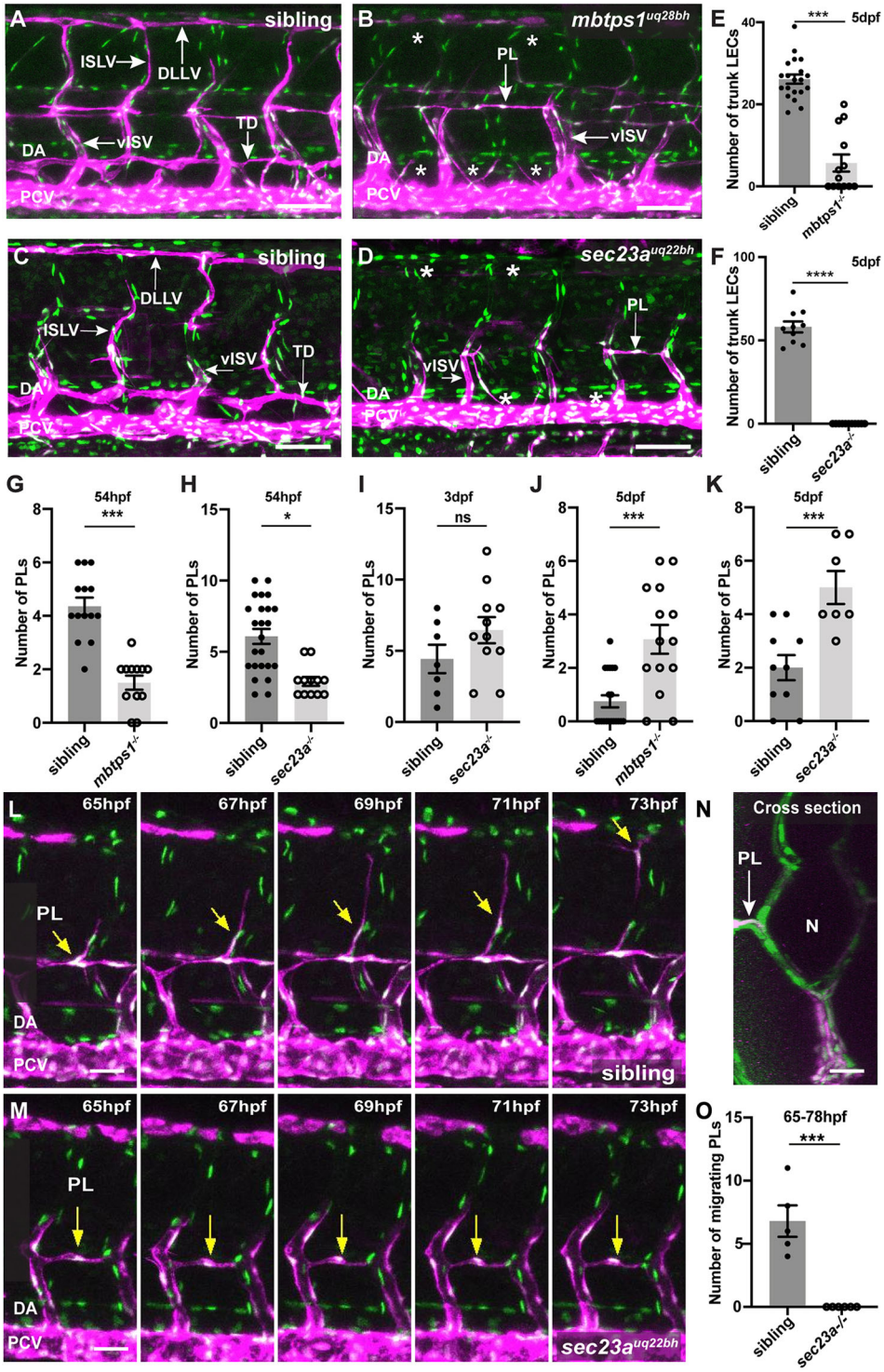

Fig. 1. *mbtps1*^{uq28bh} and *sec23a*^{uq22bh} embryos fail to form a lymphatic network in the trunk. (A-D) Confocal images of *Tg(fli1a:nEGFP); Tg(-5.2lyve1b:dsRed)* (green/magenta) sibling (A,C), *mbtps1*^{uq28bh} (B) and *sec23a*^{uq22bh} (D) embryos at 5 dpf showing *mbtps1*^{uq28bh} and *sec23a*^{uq22bh} lack TD, DLLV and ISLVs at 5 dpf. Absence indicated by asterisks. All embryos show normal development of DA, PCV and vISV at 5 dpf. (E,F) Quantification reveals fewer LECs within vessels in *mbtps1*^{uq28bh} (E) and *sec23a*^{uq22bh} (F) when compared with siblings. Measured across five somites (E) and eight somites (F). (G,H) At 54 hpf, there are fewer PLs at the HM in *mbtps1*^{uq28bh} (G) and *sec23a*^{uq22bh} (H) mutants when compared with siblings (measured across five somites). (I) At 3 dpf, there are no significant differences in the number of PLs at the HM of *sec23a*^{uq22bh} mutants when compared with siblings (measured across five somites). (J,K) At 5 dpf there are significantly more PLs at the HM in *mbtps1*^{uq28bh} (J) and *sec23a*^{uq22bh} (K) mutants when compared with siblings (measured across five somites). (L,M) Time-lapse imaging of *Tg(fli1a:nEGFP); Tg(-5.2lyve1b:dsRed)* showing PLs migrate from the HM in siblings (representative of n=7 embryos analysed) when compared with *sec23a*^{uq22bh} mutants (representative of n=4 embryos analysed). Yellow arrow indicates migrating PL (L) and stalled PL (M). (N) Cross-section showing PLs migrate adjacent to notochord. (O) There were significantly fewer PLs migrating in *sec23a*^{uq22bh} mutants (n=4) when compared with siblings (n=7). ns, not significant. *P<0.05, ***P<0.001, ****P<0.0001 (two-tailed unpaired Student's t-test). DA, dorsal aorta; DLLV, dorsal longitudinal lymphatic vessel; ISLVs, intersegmental lymphatic vessels; N, notochord; PCV, posterior cardinal vein; PL, parachordal LEC; TD, thoracic duct; vISV, venous intersegmental vessel. Scale bars: 50 µm in A-D,L,M; 80 µm in N.

Development (2020) 147, dev190983. doi:10.1242/dev.190983

mutants and cell autonomy studies suggest that Col2a1 is essential to regulate a discrete step in LEC migration and represents a key and spatially patterned component of the ECM regulating embryonic lymphangiogenesis.

RESULTS AND DISCUSSION

mbtps1 and *sec23a* mutants fail to form a lymphatic vascular network in the trunk

In an ENU mutagenesis screen for genes involved in lymphangiogenesis (see Koltowska et al., 2015b), we identified two mutants, uq^{27bh} and uq^{22bh}, that displayed craniofacial defects, a short body axis and loss of lymphatic vessels at 5 days post fertilisation (dpf) (Fig. 1A-F, Figs S1A,B and S2A,B). Using a whole-genome sequencing approach to map the location of the causative genes (Koltowska et al., 2015b), we identified a region of homozygosity for the uq^{27bh} family on chromosome 18 and a C/T nonsense mutation encoding Y511* in *mbtps1* (Fig. S1C-D′). In the uq^{22bh} family, we identified a region of homozygosity on chromosome 17 and a C/T nonsense mutation encoding Q549*, predicted to disrupt the α-helical domain of *sec23a* (Fig. S2C-D′). To confirm these mutations as causative, we used CRISPR/Cas9 to generate a 1 bp insertion at position 1157 of the coding sequence of *mbtps1*, causing a frameshift and subsequent stop codon (uq^{28bh} D405*). In *sec23a,* we generated a 3 bp deletion within the codons for amino acids 532 and 533, causing the introduction of a stop codon (uq^{23bh}, Y532*). Compound heterozygous embryos for uq^{28bh};uq^{27bh} and for uq^{23bh};uq^{22bh} displayed the same phenotypes as the ENU-generated uq^{27bh} and uq^{22bh} mutants (Figs S1E-I and S2E-I). This identifies the two ENU-generated mutants as $mbtps1^{uq27bh}$ and $sec23a^{uq22bh}$.

Mbpts1 and Sec23a are both essential for the function of the coat-protein-II (COP-II) secretory pathway: the anterograde protein trafficking route which regulates the selection and packaging of protein cargo in the endoplasmic reticulum (ER) and its transport to

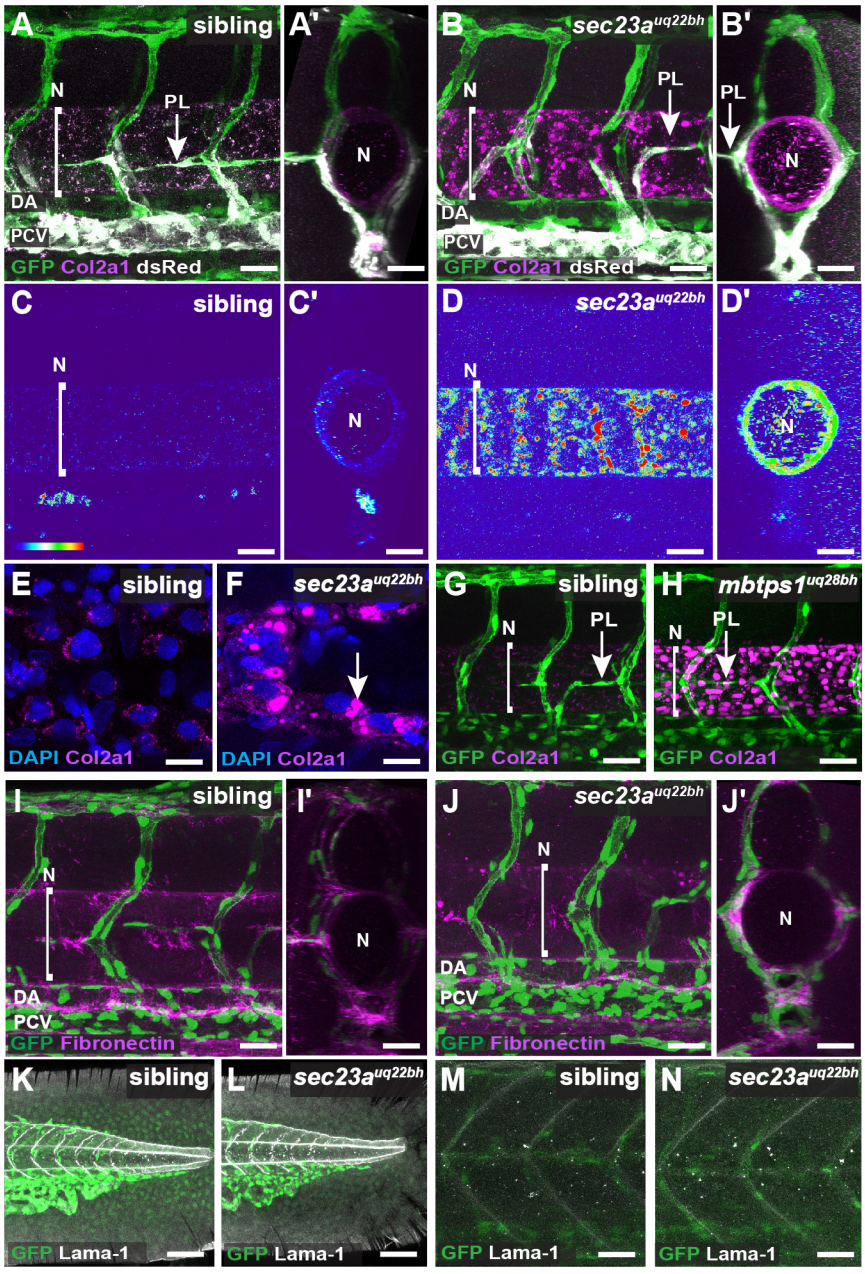

Fig. 2. *sec23a*^{uq22bh} *and mbtps1*^{uq28bh} mutant embryos display failed secretion of Collagen2a1. (A-D′) IF staining of Col2a1 and eGFP in 2 dpf *Tg(fli1a:nEGFP); Tg(-5.2lyve1b:dsRed)* siblings (A, cross-section A′) and *sec23a*^{uq22bh} mutants (B, cross-section B′) showing vasculature, secondary sprouts and Col2a1 labelled green, grey and magenta, respectively. Thermal maps showing lateral and cross sectional images reveal that *sec23a*^{uq22bh} embryos (*n*=10) exhibit an accumulation of Col2a1 around the notochord when compared with siblings (*n*=22) at 2 dpf (C-D′). (E,F) High magnification confocal images show intracellular accumulation of Col2a1 (indicated by white arrow) in NSCs in *sec23a*^{uq22bh} (F) when compared with siblings (E). (G,H) Confocal images as in A of siblings (G, *n*=12) and *mbtps1*^{uq28bh} (H, *n*=6) mutants show similar accumulation of Col2a1 at 2 dpf as *sec23a*^{uq22bh}. (I-J′) Confocal images as in A showing vasculature and secondary sprouts (green) and Fibronectin (magenta) indicate no obvious defect in secretion of Fibronectin in siblings (I, cross-section I′; *n*=36) and *sec23a*^{uq22bh} embryos (J, cross-section J′; *n*=8). (K-N) Confocal images as in A showing vasculature (green) and Laminin (Lama1; grey) indicate no obvious defect in secretion of Laminin in the fin (K,L) or somite (M,N) when siblings (*n*=36) were compared with *sec23a*^{uq22bh} mutants (*n*=7). Line marked N indicates notochord. DA, dorsal aorta; N, notochord; PCV, posterior cardinal vein. Scale bars: 100 µm in A-F; 80 µm in G-N.

Development (2020) 147, dev190983. doi:10.1242/dev.190983

the Golgi (Brandizzi and Barlowe, 2013; Szul and Sztul, 2011). The main function of Sec23a is to concentrate fully folded proteins into vesicles on the ER. Mbtps1 is a transcription factor serine protease, which cleaves and activates several transcription factors including Creb3l2 which is essential for the transcription of *sec23a* (Saito et al., 2009). Thus, both factors act in a pathway mediating ER-Golgi anterograde transport and are essential for secretion of protein cargos.

mbtps1^{uq28bh} and *sec23a*^{uq22bh} mutants were further examined on a transgenic background labelling vascular nuclei *Tg(fli1a:nEGFP)*, veins and lymphatics *Tg(-5.2lyve1b:dsRed)*. To understand when defects in lymphangiogenesis first arose, we quantified the number of PLs located in the HM at 54 hpf and 5 dpf. Both *mbtps1*^{uq28bh} and *sec23a*^{uq22bh} mutants showed a reduction in initial PL numbers in the HM (Fig. 1G,H), but at later stages PL numbers recovered (Fig. 1I), suggesting a delay in colonising the HM. Subsequently, PLs accumulated in the HM in mutants, suggesting eventual trapping of PLs (Fig. 1J,K). The formation of vISVs remained unaffected in both mutants at 54 hpf, suggesting specificity in this trunk lymphatic phenotype (Figs S1M and S2M).

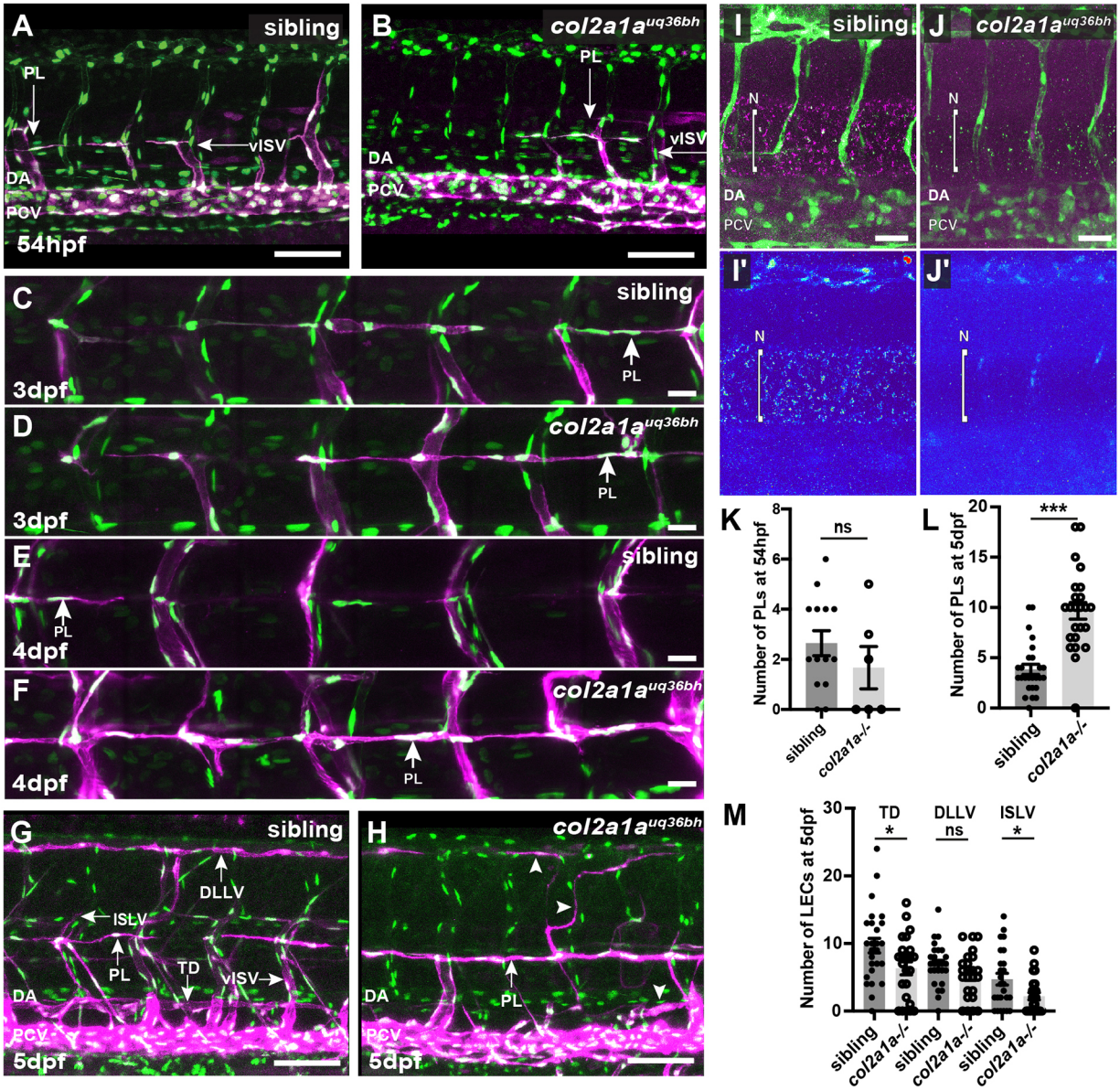

Fig. 3. *col2a1a*^{uq36bh} mutants exhibit increased PL numbers in the HM over time and reduced numbers of LECs in mature vessels. (A,B) Confocal images of *Tg(fli1a:nEGFP); Tg(-5.2lyve1b:dsRed)* sibling (A, *n*=16) and *col2a1a1*^{uq36bh} (B, *n*=9) at 54 hpf showing PLs migrate to the HM. (C-F) Confocal images of *Tg(fli1a:nEGFP); Tg(-5.2lyve1b:DsRed)* sibling (C, *n*=4; E, *n*=7) and *col2a1a*^{uq36bh} (D, *n*=5; F, *n*=7;) embryos at 3 dpf (C,D) and 4 dpf (E,F) show that PLs fail to migrate from the HM in *col2a1a*^{uq36bh} mutants compared with the siblings. (G,H) Confocal images of sibling (G, *n*=32) and *col2a1a*^{uq36bh} (H, *n*=23) embryos at 5 dpf showing stalled PLs at the HM in *col2a1a*^{uq36bh} mutants. Arrowheads indicate vessel fragments. (I,J) IF assay of Col2a1 and eGFP in *Tg(fli1a:nEGFP); Tg(-5.2lyve1b:dsRed)* siblings (I, thermal map I′, *n*=24) and *col2a1a*^{uq36bh} (J, thermal map J′, *n*=8) mutants confirm loss of Col2a1a in *col2a1a*^{uq36bh}. (K,L) No difference in PL number was observed in *col2a1a*^{uq36bh} and siblings at 54 hpf (K); however, at 5 dpf there was a significant increase in stalled PLs at the HM in *col2a1a*^{uq36bh} mutants when compared with siblings (L). (M) Quantification of nuclei in the TD and ISLV revealed a significant reduction in *col2a1a*^{uq36bh} (*n*=23) when compared with siblings (*n*=32). Line marked N indicates notochord. ns, not significant. *P<0.05, ***P<0.001 (two-tailed unpaired Student's *t*-test). TD, thoracic duct; HM, horizontal myoseptum; ISLVs, intersegmental lymphatic vessels; N, notochord; PL, parachordal LEC. Scale bars: 50 µm in A-H; 80 µm in I,J.

Development (2020) 147, dev190983. doi:10.1242/dev.190983

The craniofacial lymphatic network displayed reduced numbers of LECs in both *mbtps1*^{uq28bh} and *sec23a*^{uq22bh} mutants. However, both mutants also have craniofacial cartilage defects (Haffter et al., 1996; Schlombs et al., 2003) that could contribute to facial LEC phenotypes, and thus these vessels were not further studied (Figs S1J-L and S2J-L). To address the potential impact of general developmental delay, we examined development of the sub-intestinal vasculature, which expands from 2-5 dpf. At 3 dpf (when *sec23a* mutants already show defects in lymphangiogenesis) there was no difference in EC number in these vessels between siblings and mutants (Fig. S2N,O,R). At 5 dpf the mutants had a mildly reduced number of ECs in intestinal vessels (Fig. S2P,Q,S) but a complete loss of lymphatics, suggesting a mild general delay at later stages that is unlikely to account for the severe lymphatic defects.

Lymphangiogenesis stalls during LEC migration in *sec23a* mutants

We next investigated the timing of PL accumulation in the HM. We time-lapse imaged PLs in *sec23a*^{uq22bh} mutants and wild-type siblings from 65 hpf to 78 hpf (Movies 1 and 2). We found that although sibling PLs migrated dorsally and ventrally out of the HM during this period (Fig. 1L,N,O), mutant PLs failed to migrate out of the HM (Fig. 1M,O). These data suggest that PLs in *sec23a*^{uq22bh} mutants stall or exhibit a block in their normal migration route. As motoneurons and chemokine signalling can regulate PL migration out of the HM, we examined motoneuron development using immunofluorescence (IF) and expression of the chemokines *cxcl12a* and *cxcl12b* at the level of transcription, but found no differences in *sec23a*^{uq22bh} mutants or siblings (Fig. S3A-H). At earlier stages of development, we also found that Vegfc/Flt4 signalling was active in both mutants and siblings using IF analysis of downstream ERK-signalling (pErk1/2), and the downstream marker of LEC specification, Prox1, was also unchanged (Fig. S4A-H). Together, these data suggest a defect in LEC migration in the COP-II secretory pathway mutants.

sec23a^{uq22bh} and *mbtps1*^{uq28bh} COP-II secretory pathway mutants fail to secrete Col2a1 from NSCs along the LEC migration route

Correct composition of the ECM and cell-ECM interactions are essential for vascular development (Aszodi et al., 2006; Hynes, 2007). *sec23a (crusher)* mutants, were previously shown to display reduced secretion of cartilage ECM proteins including type II Collagen (Lang et al., 2006). The zebrafish *creb3l2 (feelgood)* and *mbtps1* (*goz)* mutants, also have decreased collagen deposition and abnormal aggregates of Col2 protein respectively (Melville et al., 2011; Schlombs et al., 2003). Thus, we performed IF analysis to examine the localisation of Col2a1 (which is produced by the NSCs) at the stages when PL migration fails in *sec23a* and *mbtps1* mutants. We observed increased intracellular accumulation of Col2a1 within the NSCs of both *sec23a*^{uq22bh} and *mbtps1*^{uq28bh} mutant embryos at 54 hpf (Fig. 2A-H). *In situ* hybridisation revealed no obvious difference in *col2a1a* transcription, indicating a likely defect in protein secretion rather than increased transcript levels (Fig. S4I,J). In contrast, Fibronectin and Laminin (Lama1), secretion appeared to be unaffected in *sec23a* mutants (Fig. 2I-N). The NSCs that normally secrete Col2a1 were located immediately adjacent to the HM and the migrating PLs at 2 dpf (Fig. 2B,B′,G,H arrows). Together, these data suggest a selective defect in secretion of Col2a1 in the region of the embryo where we observe PL migration stalling (at the HM alongside the NSCs) in mutants defective in COP-II secretory pathway function.

Col2a1 is essential for the dynamic emigration of LECs from the HM

We next asked whether the loss of Col2a1 contributes to the LEC migration phenotype in *sec23a*^{uq22bh} and *mbtps1*^{uq28bh} mutants. We generated a *col2a1a*^{uq36bh} mutant using CRISPR-mediated genome editing. The specific mutation introduced a 3 bp deletion and 4 bp insertion at position 637 of the coding sequence, predicted to cause a frameshift and subsequent stop codon, E235* (Fig. S4K,L). The *col2a1a*^{uq36bh} mutant displayed a shortened body axis (Fig. S4M, N), a lack of Col2a1 production (Fig. 3I,J) and abnormal lymphatic vessel development (Fig. 3C-H). Analysis of the number of PLs at the HM revealed that PLs could still develop in mutant embryos at 54 hpf (Fig. 3A,B,K). However, analysis of embryos from 3-5 dpf revealed that PLs failed to emigrate from, and remained trapped in, the HM (Fig. 3C-H,L). This resulted in reduced numbers of LECs in the TD and ISLVs (Fig. 3M).

To further understand the timing of Col2a1 function in LEC migration, we analysed the cellular defects in these mutants using high resolution, high-speed, time-lapse imaging of PL migration from 60-80 hpf (Movie 3). We found that, although PL migration occurred along the HM [anterior-posterior (a-p) axis], this was at a reduced velocity, indicating that PL motility was reduced (Fig. 4A, B). Quantification of the sphericity of PL nuclei (as a proxy for polarity and cell motility) showed no difference at 3 and 4 dpf, suggesting that cells polarise but have defects in migration (Fig. 4C). Analysis of migration on the embryonic dorso-ventral (d-v) axis revealed significantly less migration in mutants in comparison with siblings (Fig. 4D-H). This data indicates that, although mutant LECs maintain polarity in the HM, a lack of Col2a1 is sufficient to inhibit their ability to migrate dorsally and ventrally from the HM. Of note, the data also demonstrated significant variation in individual PL behaviours (Fig. 4G,H) indicating that some mutant cells migrate while others are severely impaired: overall a milder phenotype than in the COP-II mutants. This suggests contributions from other COP-II-dependent protein cargos, although Col2a1 clearly plays a key functional role.

Finally, to confirm that the cells contributing to the *sec23a*^{uq22bh} and *col2a1a*^{uq36bh} mutant phenotypes were the same, we injected a Tol2 DNA construct that drove expression of *sec23a* from the *col2a1a* promoter (*col2a1a:Sec23a.T2A.eGFP*). As previously reported, using this construct we were able to observe expression by the presence of EGFP specifically in the NSCs (Cox et al., 2018). Injected *sec23a* mutant embryos selected for the presence of EGFP-expressing NSCs had a partial rescue of lymphatic vessel development compared with siblings. Injected sibling and mutant embryos selected for the presence of EGFP-expressing NSCs also developed ectopic *lyve1b*-positive vessels in regions adjacent to EGFP expression around the notochord (Fig. 4I-N). The formation of ectopic vessel fragments contributed to a reduction in TD formation in siblings (Fig. 4I-N). These data indicate that secretion from the NSCs can partially restore lymphangiogenesis in *sec23a* mutants and, furthermore, that increased *sec23a* in NSCs can induce local ectopic vessel formation. Taken together with our findings above, this suggests that a defect in secretion of Col2a1 by NSCs along the LEC migration route contributes to the severe lymphatic phenotype in COP-II secretory pathway mutants (Fig. 4O,P).

Conclusion

Using a forward genetic screen, we find that, in addition to previously reported phenotypes, *mbtps1* and *sec23a* mutants exhibit a loss of the lymphatic network in the trunk. Although these COP-II

Development (2020) 147, dev190983. doi:10.1242/dev.190983

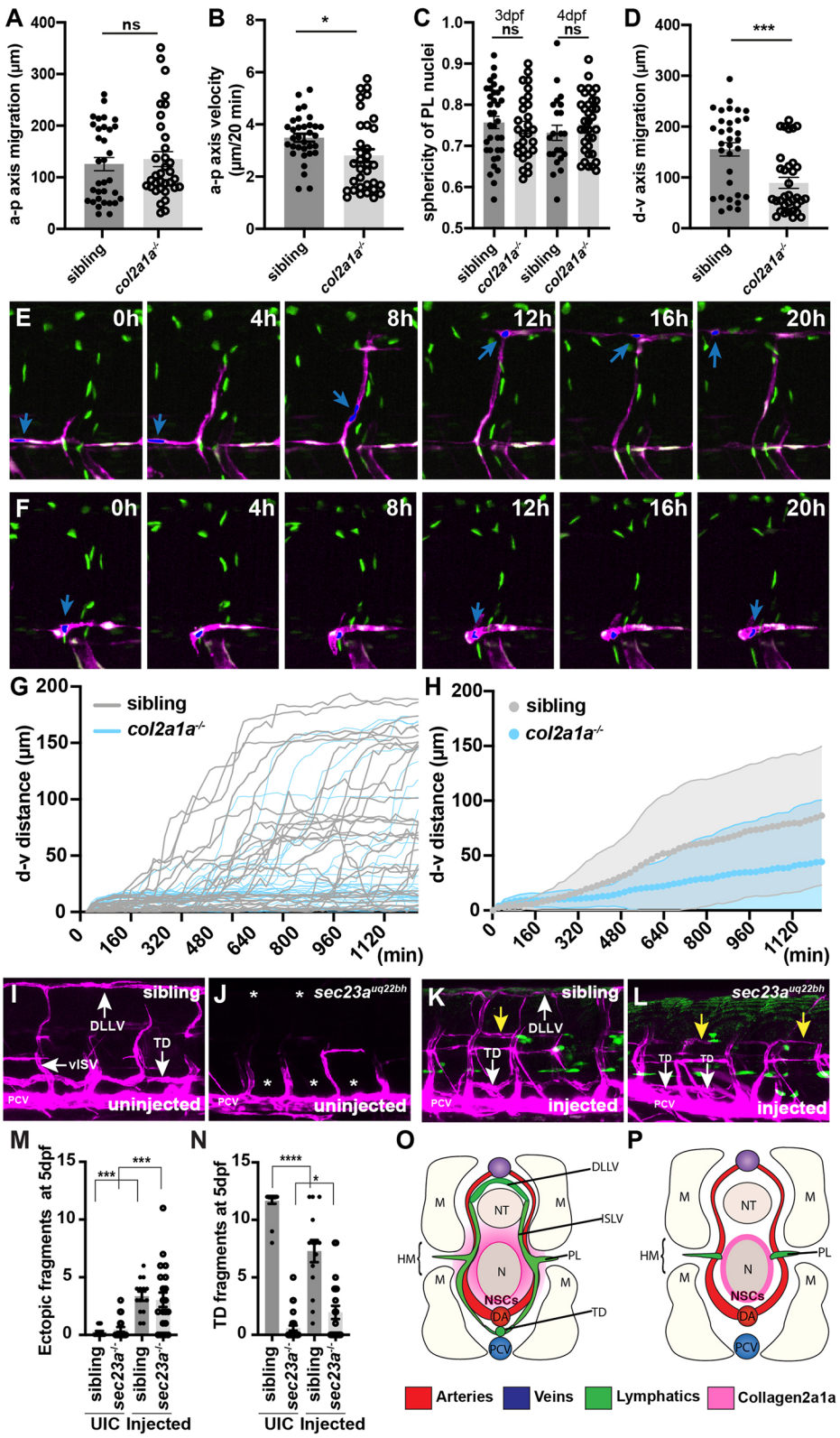

Fig. 4. Abnormal migratory dynamics of PLs underpins an absence of lymphatic vessels in *col2a1a*^{uq36bh} mutant embryos. (A) Quantification of migration distance along the anterior-posterior (a-p) axis for mutant and sibling PLs (*n*=6 embryos). (B) Quantification of the anterior-posterior (a-p) axis PL migration velocity over 20 min in sibling and mutant embryos (*n*=6 embryos). (C) Quantification of the sphericity of PL nuclei in μm^2 at 3 dpf and 4 dpf in *col2a1a*^{uq36bh} mutants compared with siblings. (D) Quantification of the dorso-ventral axis migration for sibling and mutant PLs (*n*=6 embryos). (E,F) Time-lapse imaging from 60 to 80 hpf of *Tg(fli1a:nEGFP); Tg(-5.2lyve1b:dsRed)* showing a PL migrating from the HM in siblings (*n*=6) compared with *col2a1a*^{uq36bh} mutants (*n*=6). The nuclei of a migrating (E) and stalled (F) PL are rendered blue (and indicated by blue arrow). (G,H) Quantification of dorso-ventral migration showing individual cell tracks (G) and mean±s.d. (H) for sibling and *col2a1a*^{uq36bh} PLs. (I-L) Confocal images of *Tg(-5.2lyve1b:dsRed)* (magenta) in uninjected siblings (I, *n*=20) compared with *sec23a*^{uq22bh} mutants (white asterisks, J, *n*=29) and embryos injected with *pDest:Col2a1:sec23a-p2a-EGFP* (green) (K,L). *sec23a*^{uq22bh} mutants displayed a partial rescue of TD development (white arrows) (L, *n*=21). Injected siblings (K, *n*=14) and *sec23a*^{uq22bh} mutants showed formation of ectopic vessels (yellow arrows). (M) Quantification of ectopic fragment formation in injected embryos compared with uninjected controls for both sibling and *sec23a*^{uq22bh} mutants. (N) Quantification of TD formation in *sec23a*^{uq22bh} mutants injected with *col2a1a-Sec23a-T2A-eGFP*. In siblings, the formation of ectopic fragments leads to reduced TD formation. (O,P) Schematic showing a model for Col2a1 secretion from NSCs into the ECM around the migrating PLs (O). Defects in Col2a1 secretion from NSCs leads to failed migration of PLs (P). ns, not significant. *P<0.05, ***P<0.001, ****P<0.0001 (two-tailed unpaired Student's *t*-test). HM, horizontal myoseptum; M, myotome; N, notochord; NT, neural tube; PL, parachordal LEC.

components have general roles in protein secretion, we find that at the developmental stages analysed, these mutants display a selective defect in Col2a1 secretion from NSCs. This work identifies that NSCs produce Col2a1 to support LEC migration in the embryo in a spatially regulated and restricted manner. This adds to other known molecular mechanisms involving cell-cell and cell-matrix interactions during PL migration, including chemokine signalling from arteries (Cha et al., 2012), guidance by motoneurons in the HM (Lim et al., 2011) and Ccbe1, Vegfc- and Vegfc-processing machinery produced by fibroblast-like cells and neurons (Wang et al., 2020). This work further indicates that LECs move progressively through the embryonic environment, interacting in a

Development (2020) 147, dev190983. doi:10.1242/dev.190983

'relay' with cells and matrix components as they go, to ultimately achieve normal developmental lymphangiogenesis. It seems likely that patterned deposition of matrix components along LEC migration routes could play broader roles in lymphangiogenesis in different vessel beds in both developmental and pathological settings.

MATERIALS AND METHODS

Zebrafish

All zebrafish transgenic strains *Tg(fli1a:nEGFP)*^{y7} (Lawson and Weinstein, 2002), *Tg(lyve1:DsRed)*^{nz101} (Okuda et al., 2012), *Tg(kdrl:gfp)*^{s843} (Jin et al., 2005) were maintained in accordance with the animal ethics guidelines of the University of Queensland. The forward genetic screen and whole-genome sequence mapping were performed as previously described (Koltowska et al., 2015a).

CRISPR-genome editing

CRISPR-genome editing of *sec23a, mbtps1* and *col2a1a* was performed as previously described (Gagnon et al., 2014). The guide RNA (gRNA) sequences for *sec23a* and *mbtps1* were designed using the Zhang laboratory software (http://crispr.mit.edu) and the CRISPR-scan software (http://www.crisprscan.org) was used for designing the gRNA for *col2a1a*. Both *sec23a* and *mbtps1* gRNAs were transcribed using the Ambion Megascript SP6 promoter kit (AM13301502034), whereas *col2a1a* gRNA transcription was performed using the T7 Megascript™ high yield transcription kit (Invitrogen, AM1354). gRNA clean-up was performed using the RNA clean & concentrator™ (Zymoresearch, R1015) and the gRNA sequences are provided in Table S1.

Injections and genotyping

We mixed 1 µl of *sec23a*, *mbtps1* and *col2a1a* gRNA (300 ng/µl) with 1 nl of Cas9 mRNA (1 µg/µl) transcribed from pTST3-nCas9 (Jao et al., 2013) and 1 nl injected into the yolk of one-cell-stage embryos (Table S1). DNA extraction and identification of fish harbouring and transmitting lesions was achieved using high-resolution melt analysis (HRMA) as previously described (Dahlem et al., 2012). *sec23a*^{uq22bh} siblings and mutants were genotyped using a KASP assay (LGC Genomics). Primer blast was used to design HRMA and sequencing primers, which are listed in Table S1. The *Tg(-1.7col2a1a:sec23a-v2a-EGFP)* construct was kindly provided by the Knapik lab (Cox et al., 2018) and 100 pg was co-injected with Tol2 transposase RNA as previously described (Koltowska et al., 2015a).

Whole-mount *in-situ* hybridization

Whole-mount *in-situ* hybridization (WISH) riboprobe templates for sec*23a* and *col2a1a* were amplified by PCR (Table S1.). Probes targeting *cxcl12a* and *cxcl12b* were used as previously described (Cha et al., 2012). The amplified product was gel purified (Zymoclean gel DNA recovery kit) and the DIG-incorporated RNA probe was transcribed by T3 RNA polymerase for 4 h at 37°C and purified with the RNA clean & concentrator™ kit (Zymoresearch, R1015). WISH was performed as previously described (Kartopawiro et al., 2014).

Whole-mount immunohistochemistry

Dechorionated embryos were fixed in 4% paraformaldehyde (PFA) at various embryonic stages (32 hpf, 36 hpf, 2 dpf, 3 dpf, 4 dpf, 5 dpf) by placing the tubes of embryos on a rocker at 4°C overnight. Embryos were subsequently washed with 4% PFA and different protocols were followed for probing different proteins through IF staining.

Prox1 and phosphorylated-Erk (pErk)

Stage-fixed embryos were washed in 100% methanol, three times for 5 min each on ice. The following day, the embryos were incubated for 60 min in methanol on ice. Subsequently, the embryos were washed with 100% methanol on ice three times for 5 min each. The embryos were stored at −20°C in 100% methanol for a minimum of 2 days before performing IF. Embryos were equilibrated with 1× PBT (1× PBS+0.1% Tween 20) three times for 10 min each. Embryos were then incubated in PBT+30% sucrose (w/v) overnight at 4°C to cryoprotect the embryos. Embryos were equilibrated in 1×PBT three times for 10 min each. Subsequently, the embryos were incubated in 150 mM Tris-HCl (pH 9.0) diluted in milliQ water (MQ) for 5 min at room temperature (RT) followed by an incubation at 70°C for 15 min to facilitate antigen retrieval. The embryos were then washed in 1× PBT twice for 10 min each; followed by a wash in distilled water (dH_2O) twice, for 5 min each. The water was removed and ice-cold acetone was added to the embryos, which were incubated at −20°C for 20 min. After removing acetone, embryos were washed once with 1× PBT before adding Proteinase-K (10 mg/µl, #25530015, Invitrogen). For embryos at 32 hpf Proteinase-K treatment was not required, whereas embryos at 36 hpf were incubated in Proteinase-K (1:500 dilution in 1× PBT) for 30 min without placing the embryos on a rocker. After Proteinase-K treatment, embryos were fixed in 4% PFA for 20 min at RT, without placing the embryos on a rocker. After removing Proteinase-K, the embryos were washed five times in 1× PBT for 5 min each on a rocker. Embryos were then washed once in 1× cold wash buffer made up of TBS (pH 7.6), 0.1% Triton X-100. Embryos were then transferred into the 0.5 ml Eppendorf tubes using a Pasteur pipette. TBST was made using 10× TBS (pH 7.6), 10% Triton X-100 diluted in MQ. The blocking solution was made with TBS (pH 7.6), 0.1% Triton X-100, 1% bovine serum albumin (BSA) and 10% horse heat inactivated serum, and used to incubate embryos overnight on a rocker at 4°C. Subsequently, embryos were incubated with primary antibodies anti-GFP (1:250, #ab13970, Abcam), anti-Prox1 (1:250, # 11-002, AngioBio) and phospho-p44/42 MAPK (Erk1/2) antibody (1:250, # 4370, Cell Signaling Technology) diluted in the blocking solution on a rocker at 4°C overnight. Embryos were subsequently washed in TBST/0.1% Triton X-100 (wash buffer) five times for 30 min each, placed in a rocker at RT. The embryos were later washed in Maleic buffer [150 mM Maleic acid, 100 mM NaCl, 0.001% Tween20 (pH 7.4) saturated with 10N NaOH] once for 30 min at RT. Embryos in 2% blocking reagent (#11096176001, Roche Applied Sciences) diluted in Maleic buffer were placed on a rocker at RT for 3 h. Embryos were incubated on a rocker overnight in 4°C in the secondary fluorescence-conjugated antibodies Alexa 488 (1:400, #A11039, Invitrogen) and HRP-conjugated secondary antibody (1:1000, #W4011, Promega) diluted in Maleic buffer and 2% blocking reagent. The following day, embryos were washed five times in Maleic buffer for 30 min each at RT on a rocker. Embryos were washed once in 1× PBS and incubated in TSA Plus reaction solution (1:50 dilution of Cy3 in 1× amplification diluent; Perkin Elmer) at RT for 3 h. Embryos were washed in TBS (pH 7.6), 0.1% Triton X-100 wash buffer for at least 2 days before imaging.

Collagen type II, Fibronectin and Laminin

Embryos were fixed overnight in 4% PFA at 4°C, washed five times in PBST (PBS with 0.2% Triton X-100) and incubated in DNAse I buffer [66 mM Tris (pH 7.5), 5 mM $MgCl_2$, 1 mM 2-Mercaptoethanol, 50 U/ml DNAse I in PBST] at 37°C for 75 min. Embryos were incubated in Proteinase-K (1:1000) for 20 min at RT followed by blocking for 60 min in blocking solution (1% Triton X-100, 10% horse heat inactivated serum, 1% DMSO, 100 mM maleic acid in PBS). Embryos were incubated with the primary antibodies anti-collagen type II (1:200, #II-II6B3, Developmental Studies Hybridoma Bank); anti-laminin-a (1:250, L9693, Sigma-Aldrich), anti-living colors DsRed (1:500, 623496-100UL, Fisher Scientific) and anti-GFP (1:250, #ab13970, Abcam), diluted in blocking solution overnight at 4°C. They were then washed six times for 30 min in wash solution (1% DMSO, 100 mM maleic acid in 0.2% PBST) and incubated with fluorescence-conjugated secondary antibodies Alexa 488 (1:400, #A11039, Invitrogen), Alexa 546 (1:500, #A11010, Invitrogen), Alexa 647 (1:300, #A21240, Invitrogen) and DAPI (1:1000, #D9542-10MG, Sigma-Aldrich) in blocking solution overnight at 4°C. Embryos were washed in PBST six times for 30 min each and imaged. IF assays on the embryos for fibronectin were also fixed in 4% PFA and washed five times in PBST (PBS with 0.3% Triton X-100). Embryos were incubated in Proteinase-K (1:500) for 20 min at RT followed by blocking overnight in blocking solution (4% BSA, 10% DMSO, 0.1% PBS-Triton X-100). Embryos were incubated with primary antibodies: anti-GFP (1:250, #ab13970, Abcam) and anti-fibronectin (1:300, #F3638, Sigma-Aldrich) diluted in blocking solution overnight at 4°C. They were then washed three times for 1 h each in 0.3% Triton X-100/PBS with 1% DMSO. After

Development (2020) 147, dev190983. doi:10.1242/dev.190983

embryos were blocked for 1 h in blocking buffer, embryos were incubated with fluorescence-conjugated secondary antibodies Alexa 488 (1:400, #A11039, Invitrogen) and Alexa 647 (1:300, #A21240, Invitrogen) in blocking solution overnight at 4°C. Embryos were washed three times for 1 h each in 0.3% Triton X-100/PBS, fixed in 4% PFA at RT for a maximum of 2 h and washed several times in 0.3% Triton X-100/PBS before imaging.

Acetylated-tubulin

Embryos were fixed in 4% PFA at 4°C overnight, and rinsed in a methanol series of 75%, 50% and 25% diluted in PBST (PBS with 0.3% Triton X-100) for 10 min each, followed by three washes in PBST for 5 min each. The embryos were incubated in the blocking solution (10% horse heat inactivated serum in PBST) for 1 h at RT on a rocker. The embryos were then incubated overnight on a rocker at 4°C with primary antibodies anti-GFP (1:250, #ab13970, Abcam) and anti-tubulin (1:200, #T6793, Sigma-Aldrich) diluted in the blocking solution. The next day, the embryos were washed three times in PBST for 1 h each followed by an incubation in the blocking buffer for 1 h at RT on a rocker. The embryos were then incubated in fluorescent-conjugated secondary antibodies Alexa 488 (1:400, #A11039, Invitrogen) and Alexa 647 (1:300, #A21240, Invitrogen) diluted in the blocking buffer overnight at 4°C on a rocker. The following day, embryos were washed in PBST three times for 1 h followed by re-fixation of the embryos in 4% PFA for 30 min. The embryos were then washed in PBST three times for 5 min before imaging.

Alcian blue staining

After fixing embryos overnight in 4% PFA at 4°C the embryos were washed in 1× PBT (PBS with 0.1% Tween-20) three times for 5 min on a rocker. Embryos were incubated in Alcian Blue solution [0.1% Alcian Blue (w/v) in 80% ethanol and 20% glacial acetic acid, filtered through a 0.2 µm syringe filter before use] at RT for 6 h. Embryos were washed in an ethanol series of 75%, 50% and 25% diluted in in PBT (PBS with 0.1% Tween-20) for 5 min each. Embryos were then incubated in bleach solution (3% hydrogen peroxide and 1% potassium hydroxide diluted in PBT) at RT for 2 h in 2 ml Eppendorf tubes with caps open to facilitate removal of pigments from the embryos. The embryos were then washed in PBT for 5 min before imaging.

Imaging and quantification

Embryos were mounted laterally on 0.7% low melting temperature agarose (Sigma-Aldrich, A9414-100G) and imaged on a Zeiss LSM 710 FCS confocal microscope or an Andor dragonfly spinning disc confocal microscope with the Zyla 4.2 sCMOS camera (exclusively for Movie 3). All images were processed using Fiji software (Schindelin et al., 2012) and time-lapse movies were processed in Imaris (Bitplane). Quantification of LEC number was performed across specific somites specified in the figure legends as previously described (Koltowska et al., 2015b) by quantifying the nuclei in *z*-stacks of confocal micrographs using the *Tg(fli1a:nEGFP) Tg(-5.2lyve1b:DsRed)* transgenic line. The sphericity of PL nuclei in Fig. 4 was generated using the Spot detection algorithm from Imaris (Bitplane).

Statistical analysis

Statistical analysis was performed using Prism software (GraphPad software) using the two-tailed unpaired Student's *t*-test for all statistical analysis. Error bars indicate s.e.m. *P*-values are represented as $*P<0.05$, $**P<0.01$, $***P<0.001$, $****P<0.0001$.

Acknowledgements

The Institute for Molecular Bioscience (IMB) Sequencing Facility performed all sequencing. Imaging was performed in the Australian Cancer Research Foundation's Cancer Ultrastructure and Function Facility at IMB.

Competing interests

The authors declare no competing or financial interests.

Author contributions

Conceptualization: S.C., K.S.O., B.M.H., N.I.B.; Software: G.J.B., C.S.; Formal analysis: G.J.B., C.S.; Investigation: S.C., K.S.O., K.K., A.K.L., S.P., K.A.S., N.I.B.; Writing - original draft: S.C., B.M.H., N.I.B.; Writing - review & editing: B.M.H., N.I.B.; Supervision: B.M.H., N.I.B.

Funding

This work was supported in part by Australian Research Council discovery grants (DP150103110 and DP180102846). A.K.L. was supported by a University of Queensland Postdoctoral Fellowship. K.K. was supported by a Lymphatic Education & Research Network Postdoctoral Fellowship. K.A.S. was part funded by an Australian Research Council Future Fellowship (FT110100496). B.M.H. was supported by fellowships from the National Heart Foundation and National Health and Medical Research Council (1083811 and 1155221).

Supplementary information

Supplementary information available online at
https://dev.biologists.org/lookup/doi/10.1242/dev.190983.supplemental

References

Aszodi, A., Legate, K. R., Nakchbandi, I. and Fässler, R. (2006). What mouse mutants teach us about extracellular matrix function. *Annu. Rev. Cell Dev. Biol.* **22**, 591-621. doi:10.1146/annurev.cellbio.22.010305.104258

Bazigou, E., Xie, S., Chen, C., Weston, A., Miura, N., Sorokin, L., Adams, R., Muro, A. F., Sheppard, D. and Makinen, T. (2009). Integrin-alpha9 is required for fibronectin matrix assembly during lymphatic valve morphogenesis. *Dev. Cell* **17**, 175-186. doi:10.1016/j.devcel.2009.06.017

Brandizzi, F. and Barlowe, C. (2013). Organization of the ER-Golgi interface for membrane traffic control. *Nat. Rev. Mol. Cell Biol.* **14**, 382-392. doi:10.1038/nrm3588

Bussmann, J., Bos, F. L., Urasaki, A., Kawakami, K., Duckers, H. J. and Schulte-Merker, S. (2010). Arteries provide essential guidance cues for lymphatic endothelial cells in the zebrafish trunk. *Development* **137**, 2653-2657. doi:10.1242/dev.048207

Cha, Y. R., Fujita, M., Butler, M., Isogai, S., Kochhan, E., Siekmann, A. F. and Weinstein, B. M. (2012). Chemokine signaling directs trunk lymphatic network formation along the preexisting blood vasculature. *Dev. Cell* **22**, 824-836. doi:10.1016/j.devcel.2012.01.011

Cox, N. J., Unlu, G., Bisnett, B. J., Meister, T. R., Condon, B. M., Luo, P. M., Smith, T. J., Hanna, M., Chhetri, A., Soderblom, E. J. et al. (2018). Dynamic glycosylation governs the vertebrate COPII protein trafficking pathway. *Biochemistry* **57**, 91-107. doi:10.1021/acs.biochem.7b00870

Dahlem, T. J., Hoshijima, K., Jurynec, M. J., Gunther, D., Starker, C. G., Locke, A. S., Weis, A. M., Voytas, D. F. and Grunwald, D. J. (2012). Simple methods for generating and detecting locus-specific mutations induced with TALENs in the zebrafish genome. *PLoS Genet.* **8**, e1002861. doi:10.1371/journal.pgen.1002861

Danussi, C., Spessotto, P., Petrucco, A., Wassermann, B., Sabatelli, P., Montesi, M., Doliana, R., Bressan, G. M. and Colombatti, A. (2008). Emilin1 deficiency causes structural and functional defects of lymphatic vasculature. *Mol. Cell. Biol.* **28**, 4026-4039. doi:10.1128/MCB.02062-07

Davis, G. E. and Camarillo, C. W. (1996). An α2β1 integrin-dependent pinocytic mechanism involving intracellular vacuole formation and coalescence regulates capillary lumen and tube formation in three-dimensional collagen matrix. *Exp. Cell Res.* **224**, 39-51. doi:10.1006/excr.1996.0109

De Angelis, J. E., Lagendijk, A. K., Chen, H., Tromp, A., Bower, N. I., Tunny, K. A., Brooks, A. J., Bakkers, J., Francois, M., Yap, A. S. et al. (2017). Tmem2 regulates embryonic Vegf signaling by controlling hyaluronic acid turnover. *Dev. Cell* **40**, 421. doi:10.1016/j.devcel.2017.02.005

Frye, M., Taddei, A., Dierkes, C., Martinez-Corral, I., Fielden, M., Ortsäter, H., Kazenwadel, J., Calado, D. P., Ostergaard, P., Salminen, M. et al. (2018). Matrix stiffness controls lymphatic vessel formation through regulation of a GATA2-dependent transcriptional program. *Nat. Commun.* **9**, 1511. doi:10.1038/s41467-018-03959-6

Gagnon, J. A., Valen, E., Thyme, S. B., Huang, P., Akhmetova, L., Pauli, A., Montague, T. G., Zimmerman, S., Richter, C. and Schier, A. F. (2014). Efficient mutagenesis by Cas9 protein-mediated oligonucleotide insertion and large-scale assessment of single-guide RNAs. *PLoS ONE* **9**, e98186. doi:10.1371/journal.pone.0098186

Haffter, P., Granato, M., Brand, M., Mullins, M. C., Hammerschmidt, M., Kane, D. A., Odenthal, J., van Eeden, F. J., Jiang, Y. J., Heisenberg, C. P. et al. (1996). The identification of genes with unique and essential functions in the development of the zebrafish, Danio rerio. *Development* **123**, 1-36.

Hogan, B. M., Bos, F. L., Bussmann, J., Witte, M., Chi, N. C., Duckers, H. J. and Schulte-Merker, S. (2009). Ccbe1 is required for embryonic lymphangiogenesis and venous sprouting. *Nat. Genet.* **41**, 396-398. doi:10.1038/ng.321

Hogan, B. M. and Schulte-Merker, S. (2017). How to plumb a pisces: understanding vascular development and disease using zebrafish embryos. *Dev. Cell* **42**, 567-583. doi:10.1016/j.devcel.2017.08.015

Hynes, R. O. (2007). Cell-matrix adhesion in vascular development. *J. Thromb. Haemost.* **5** Suppl. 1, 32-40. doi:10.1111/j.1538-7836.2007.02569.x

Jao, L.-E., Wente, S. R. and Chen, W. (2013). Efficient multiplex biallelic zebrafish genome editing using a CRISPR nuclease system. *Proc. Natl. Acad. Sci. USA* **110**, 13904-13909. doi:10.1073/pnas.1308335110

Jeltsch, M., Jha, S. K., Tvorogov, D., Anisimov, A., Leppänen, V.-M., Holopainen, T., Kivelä, R., Ortega, S., Kärpanen, T. and Alitalo, K. (2014). CCBE1 enhances lymphangiogenesis via A disintegrin and metalloprotease with thrombospondin motifs-3-mediated vascular endothelial growth factor-C activation. *Circulation* **129**, 1962-1971. doi:10.1161/CIRCULATIONAHA.113.002779

Jin, S.-W., Beis, D., Mitchell, T., Chen, J. N. and Stainier, D. Y. (2005). Cellular and molecular analyses of vascular tube and lumen formation in zebrafish. *Development* **132**, 5199-5209. doi:10.1242/dev.02087

Joukov, V., Sorsa, T., Kumar, V., Jeltsch, M., Claesson-Welsh, L., Cao, Y., Saksela, O., Kalkkinen, N. and Alitalo, K. (1997). Proteolytic processing regulates receptor specificity and activity of VEGF-C. *EMBO J.* **16**, 3898-3911. doi:10.1093/emboj/16.13.3898

Karpanen, T., Padberg, Y., van de Pavert, S. A., Dierkes, C., Morooka, N., Peterson-Maduro, J., van de Hoek, G., Adrian, M., Mochizuki, N., Sekiguchi, K. et al. (2017). An evolutionarily conserved role for Polydom/Svep1 during lymphatic vessel formation. *Circ. Res.* **120**, 1263-1275. doi:10.1161/CIRCRESAHA.116.308813

Kartopawiro, J., Bower, N. I., Karnezis, T., Kazenwadel, J., Betterman, K. L., Lesieur, E., Koltowska, K., Astin, J., Crosier, P., Vermeren, S. et al. (2014). Arap3 is dysregulated in a mouse model of hypotrichosis-lymphedema-telangiectasia and regulates lymphatic vascular development. *Hum. Mol. Genet.* **23**, 1286-1297. doi:10.1093/hmg/ddt518

Koltowska, K., Lagendijk, A. K., Pichol-Thievend, C., Fischer, J. C., Francois, M., Ober, E. A., Yap, A. S. and Hogan, B. M. (2015a). Vegfc regulates bipotential precursor division and Prox1 expression to promote lymphatic identity in Zebrafish. *Cell Reports* **13**, 1828-1841. doi:10.1016/j.celrep.2015.10.055

Koltowska, K., Paterson, S., Bower, N. I., Baillie, G. J., Lagendijk, A. K., Astin, J. W., Chen, H., Francois, M., Crosier, P. S., Taft, R. J. et al. (2015b). mafba is a downstream transcriptional effector of Vegfc signaling essential for embryonic lymphangiogenesis in zebrafish. *Genes Dev.* **29**, 1618-1630. doi:10.1101/gad.263210.115

Lang, M. R., Lapierre, L. A., Frotscher, M., Goldenring, J. R. and Knapik, E. W. (2006). Secretory COPII coat component Sec23a is essential for craniofacial chondrocyte maturation. *Nat. Genet.* **38**, 1198-1203. doi:10.1038/ng1880

Lawson, N. D. and Weinstein, B. M. (2002). In vivo imaging of embryonic vascular development using transgenic zebrafish. *Dev. Biol.* **248**, 307-318. doi:10.1006/dbio.2002.0711

Le Guen, L., Karpanen, T., Schulte, D., Harris, N. C., Koltowska, K., Roukens, G., Bower, N. I., van Impel, A., Stacker, S. A., Achen, M. G. et al. (2014). Ccbe1 regulates Vegfc-mediated induction of Vegfr3 signaling during embryonic lymphangiogenesis. *Development* **141**, 1239-1249. doi:10.1242/dev.100495

Lim, A. H., Suli, A., Yaniv, K., Weinstein, B., Li, D. Y. and Chien, C. B. (2011). Motoneurons are essential for vascular pathfinding. *Development* **138**, 3847-3857. doi:10.1242/dev.068403

Lutter, S., Xie, S., Tatin, F. and Makinen, T. (2012). Smooth muscle-endothelial cell communication activates Reelin signaling and regulates lymphatic vessel formation. *J. Cell Biol.* **197**, 837-849. doi:10.1083/jcb.201110132

Ma, Q., Dieterich, L. C. and Detmar, M. (2018). Multiple roles of lymphatic vessels in tumor progression. *Curr. Opin. Immunol.* **53**, 7-12. doi:10.1016/j.coi.2018.03.018

Melville, D. B., Montero-Balaguer, M., Levic, D. S., Bradley, K., Smith, J. R., Hatzopoulos, A. K. and Knapik, E. W. (2011). The feelgood mutation in zebrafish dysregulates COPII-dependent secretion of select extracellular matrix proteins in skeletal morphogenesis. *Dis. Model. Mech.* **4**, 763-776. doi:10.1242/dmm.007625

Morooka, N., Futaki, S., Sato-Nishiuchi, R., Nishino, M., Totani, Y., Shimono, C., Nakano, I., Nakajima, H., Mochizuki, N. and Sekiguchi, K. (2017). Polydom is an extracellular matrix protein involved in lymphatic vessel remodeling. *Circ. Res.* **120**, 1276-1288. doi:10.1161/CIRCRESAHA.116.308825

Okuda, K. S., Astin, J. W., Misa, J. P., Flores, M. V., Crosier, K. E. and Crosier, P. S. (2012). lyve1 expression reveals novel lymphatic vessels and new mechanisms for lymphatic vessel development in zebrafish. *Development* **139**, 2381-2391. doi:10.1242/dev.077701

Petrova, T. V. and Koh, G. Y. (2018). Organ-specific lymphatic vasculature: from development to pathophysiology. *J. Exp. Med.* **215**, 35-49. doi:10.1084/jem.20171868

Planas-Paz, L., Strilic, B., Goedecke, A., Breier, G., Fassler, R. and Lammert, E. (2012). Mechanoinduction of lymph vessel expansion. *EMBO J.* **31**, 788-804. doi:10.1038/emboj.2011.456

Podgrabinska, S., Braun, P., Velasco, P., Kloos, B., Pepper, M. S. and Skobe, M. (2002). Molecular characterization of lymphatic endothelial cells. *Proc. Natl. Acad. Sci. USA* **99**, 16069-16074. doi:10.1073/pnas.242401399

Saito, A., Hino, S., Murakami, T., Kanemoto, S., Kondo, S., Saitoh, M., Nishimura, R., Yoneda, T., Furuichi, T., Ikegawa, S. et al. (2009). Regulation of endoplasmic reticulum stress response by a BBF2H7-mediated Sec23a pathway is essential for chondrogenesis. *Nat. Cell Biol.* **11**, 1197-1204. doi:10.1038/ncb1962

Schindelin, J., Arganda-Carreras, I., Frise, E., Kaynig, V., Longair, M., Pietzsch, T., Preibisch, S., Rueden, C., Saalfeld, S., Schmid, B. et al. (2012). Fiji: an open-source platform for biological-image analysis. *Nat. Methods* **9**, 676-682. doi:10.1038/nmeth.2019

Schlombs, K., Wagner, T. and Scheel, J. (2003). Site-1 protease is required for cartilage development in zebrafish. *Proc. Natl. Acad. Sci. USA* **100**, 14024-14029. doi:10.1073/pnas.2331794100

Seo, E., Seo, K. W., Gil, J.-E., Ha, Y.-R., Yeom, E., Lee, S. and Lee, S. J. (2014). Biophysiochemical properties of endothelial cells cultured on bio-inspired collagen films. *BMC Biotechnol.* **14**, 61. doi:10.1186/1472-6750-14-61

Szul, T. and Sztul, E. (2011). COPII and COPI traffic at the ER-Golgi interface. *Physiology (Bethesda)* **26**, 348-364. doi:10.1152/physiol.00017.2011

Wang, G., Muhl, L., Padberg, Y., Dupont, L., Peterson-Maduro, J., Stehling, M., le Noble, F., Colige, A., Betsholtz, C., Schulte-Merker, S. et al. (2020). Specific fibroblast subpopulations and neuronal structures provide local sources of Vegfc-processing components during zebrafish lymphangiogenesis. *Nat. Commun.* **11**, 2724. doi:10.1038/s41467-020-16552-7

Whelan, M. C. and Senger, D. R. (2003). Collagen I initiates endothelial cell morphogenesis by inducing actin polymerization through suppression of cyclic AMP and protein kinase A. *J. Biol. Chem.* **278**, 327-334. doi:10.1074/jbc.M207554200

Yaniv, K., Isogai, S., Castranova, D., Dye, L., Hitomi, J. and Weinstein, B. M. (2006). Live imaging of lymphatic development in the zebrafish. *Nat. Med.* **12**, 711-716. doi:10.1038/nm1427

Table S1. CRISPR and oligo sequences used for HRMA, sequencing, and whole mount *in-situ* hybridization (WISH) probe

Oligo Name	Sequence 5'-3'
sec23a gRNA	GGCCCGTCTTGCTGTGTACAAGG
sec23a^{uq23bh} HRMA FP	GCGAAAGCTTGTGTTCGAAGG
sec23a^{uq23bh} HRMA RP	CGGATGAGCTGTCTGTCCAA
sec23a^{uq23bh} sequencing FP	AATGGGGTGGTCAAAATAGGG
sec23a^{uq23bh} sequencing RP	CGAAAGCTTGTGTTCGAAGGT
col2a1a gRNA	GGAGGGGCCAGGAGGACCAC
col2a1a^{uq36bh} HRMA FP	TGGGTCAAAGATGCCATGTTGC
col2a1a^{uq36bh} HRMA RP	ATGCATTTACTTACAGGTGCTCCA
col2a1a^{uq36bh} sequencing FP	GAGGAATGTTTTGGAATGACGTGG
col2a1a^{uq36bh} sequencing RP	AGTGTGGGATTTGGGAGTTGG
mbtps1 gRNA	ACATTGCCAGGTTTTCATCC
mbtps1^{uq27bh} sequencing FP	CCTGTCACGCCCATACCATTA
mbtps1^{uq27bh} sequencing RP	CTAGCATTCTGCTCGCATCAC
mbtps1^{uq28bh} HRMA FP	GGTGTTGGAGGGATTGATTTTGAG
mbtps1^{uq28bh} HRMA RP	AAGGTGTCTGTCTGCCCTTTTTA
sec23a WISH FP	GCGCACCCATTCTGACAG
sec23a WISH RP	GGAATTAACCCTCACTAAAGGGAGAATCTCCGACCACCATGCCAG
sec23b WISH FP	CACACTTGTGAGCTTCAGGAAC
sec23b WISH RP	GGATCCATTAACCCTCACTAAAGGGAACGAACACGTAGCTCTTGGCGA

col2a1a WISH FP	TGCTGTGTGACGAGGTCAT
col2a1a WISH RP	GGAATTAACCCTCACTAAAGGGTTGCCTTGGAAACCTTGTG
cxcl12a WISH FP	AAAAAGCCCAACAGCAGCAGG
cxcl12a WISH RP	GGAATTAACCCTCACTAAAGACACGGAGCAAACAGGACTCC
cxcl12b WISH FP	ATCCTTGCTTTGTGGTCCAG
cxcl12b WISH RP	GGAATTAACCCTCACTAAAGTAGCGTTGTGTGACCAGAGG

Supplementary Figure 1

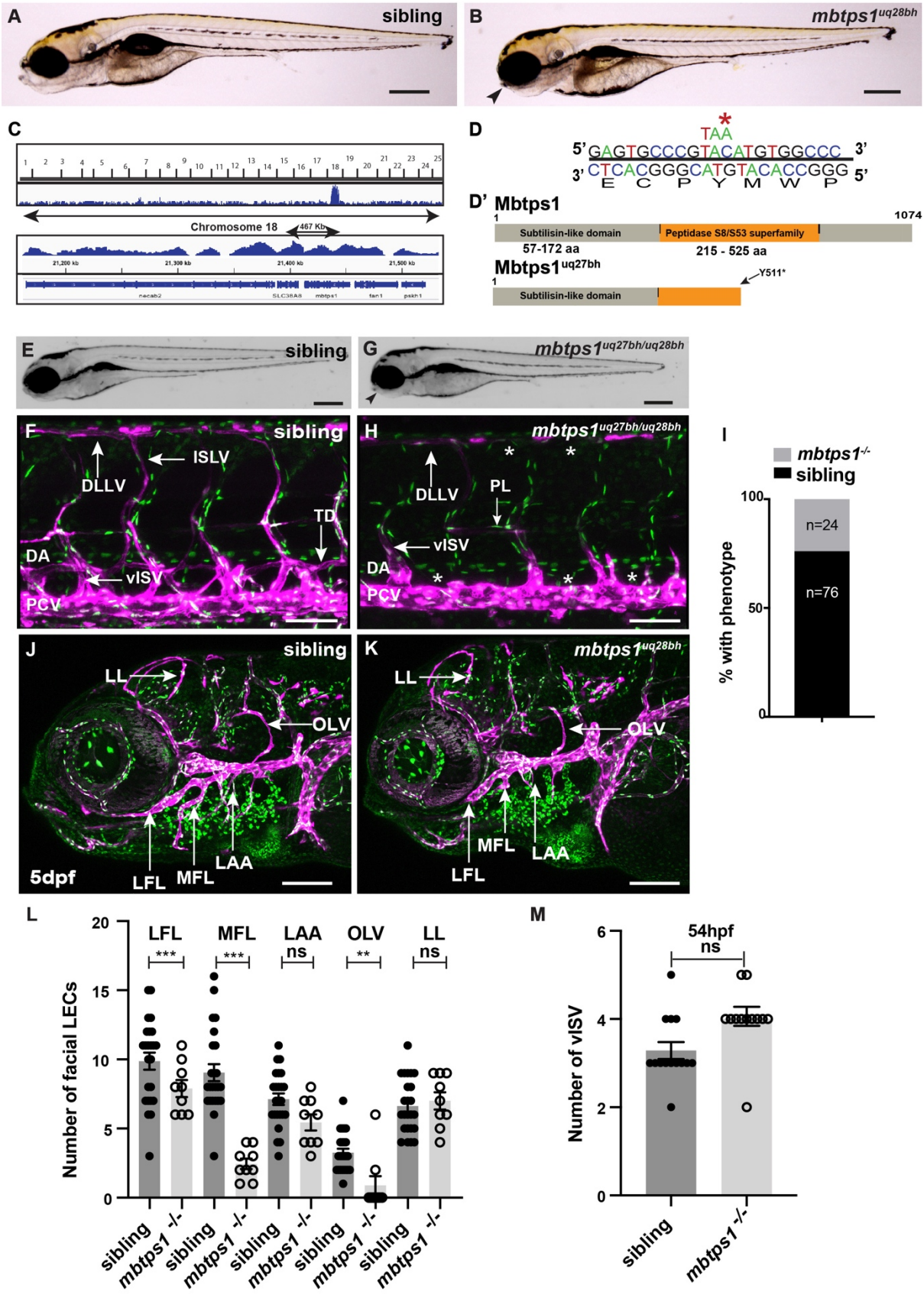

Fig. S1. Phenotyping and positional cloning of *mbtps1*^{uq27bh} using whole-genome sequence-based homozygosity mapping and mutation detection.

(A,B) Brightfield images showing shortened body axis and craniofacial defects in *mbtps1*^{uq28bh} mutant when compared to sibling at 5dpf. Black arrow indicates abnormal jaw structure. Bars, 50μm.

(C-D') Schematic plot of homozygosity across 25 chromosomes, shows a region of homozygosity on chromosome 18 containing *mbtps1* (A) with a C>A mutation introducing a premature stop codon at amino acid 511 in *mbtps1*^{uq27bh} (B, B').

(E-H) Brightfield and confocal images *Tg(fli1a:nEGFP); Tg(-5.2lyve1b:DsRed)* of sibling (E,F) and a *mbtps1*$^{uq27bh/uq28bh}$ compound heterozygous mutant (G,H). Short body axis, craniofacial defects (G) and loss of the lymphatic network (H) in compound mutants confirms *mbtps1* as the causative gene for the lymphatic defects observed at 5dpf. Bars, 50μm

(I) 24% of embryos from a complementation test showed mutant phenotype and were confirmed as compound heterozygous *mbtps1*$^{uq27bh/uq28bh}$ mutants (n=96 embryos scored).

(J-L) Confocal images *Tg(fli1a:nEGFP); Tg(-5.2lyve1b:DsRed) mbtps1*^{uq27bh} embryos. Siblings (J; n=20) display normal development of facial lymphatic vessels while *mbtps1*^{uq28bh} (K; n=6) have a significant reduction in the LFL, MFL, and at 5dpf (L). Bars, 30μm

LFL= lateral facial lymphatic; MFL= medial facial lymphatic.

(M) Quantification of vISVs at 54hpf reveals no difference between sibling (n=20) and *mbtps1*^{uq28bh} embryos (n=6). vISVs= venous intersegmental vessels.

*=P value<0.05, **=P value<0.01,***=P value<0.001.

Supplementary Figure 2

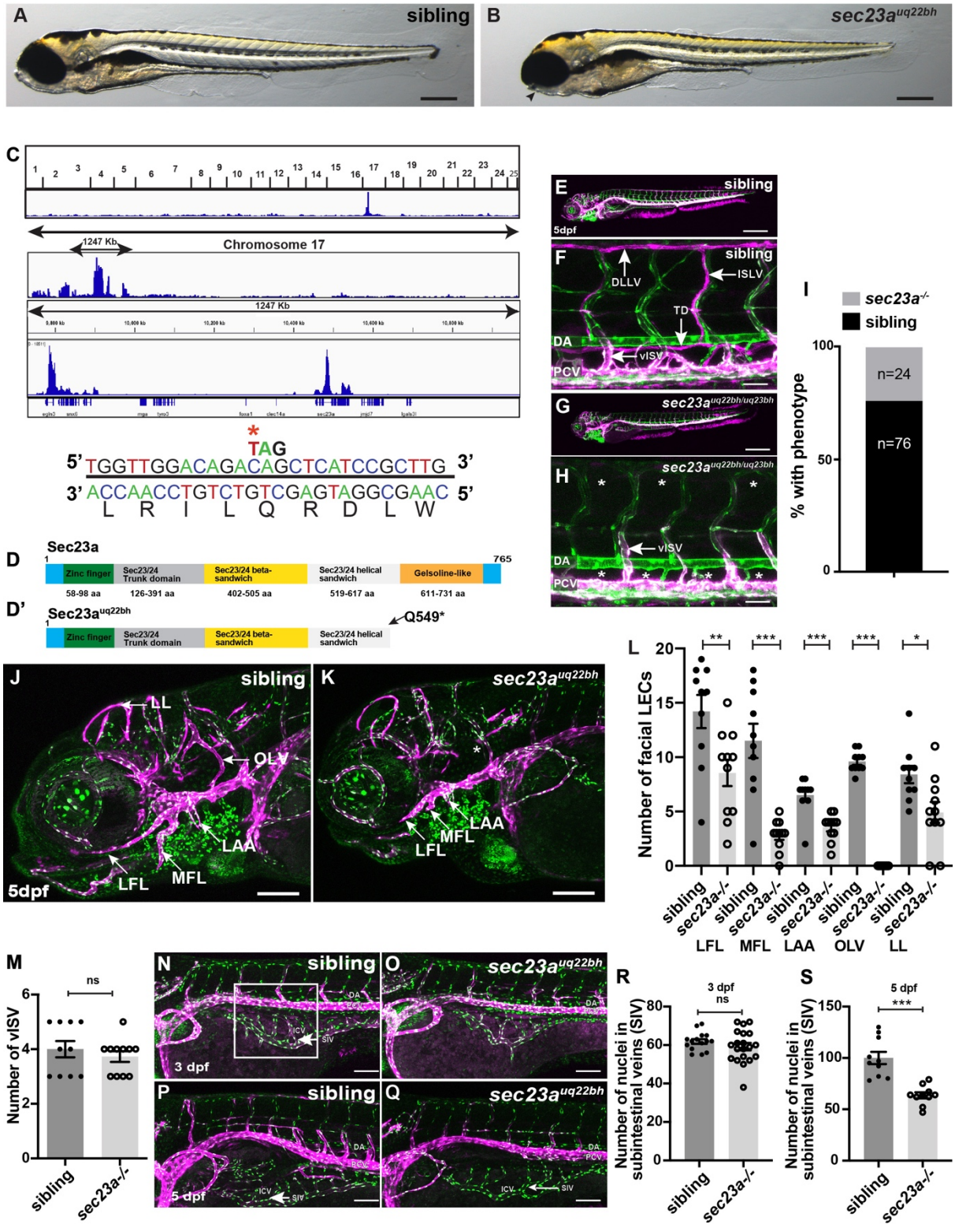

Fig. S2. Phenotyping and positional cloning of *sec23a*^{uq22bh} using whole-genome sequence-based homozygosity mapping and mutation detection.

(A,B) Brightfield images showing shortened body axis and craniofacial defects in a *sec23a*^{uq22bh} mutant when compared to sibling at 5dpf. Black arrow indicates abnormal jaw structure. Bars, 50μm.

(C-D') Schematic plot of homozygosity across 25 chromosomes, (C) shows linkage to chromosome 17 containing *sec23a*, with a C>T mutation (C) introducing a premature stop codon at amino acid 549 (D,D').

(E-H) Brightfield and confocal images of *Tg(kdrl:EGFP); Tg(-5.2lyve1b:DsRed)* sibling (E,F) and a *sec23a*$^{uq22bh/uq23bh}$ complementation test (G,H). The short body axis (G) and loss of the lymphatic network (H) in compound mutants confirms *sec23a* as the causative gene for the lymphatic defects observed at 5dpf. Bars, 50μm

(I) 24% of embryos from a complementation test showed mutant phenotype and were confirmed as compound heterozygous *sec23a*$^{uq22bh/uq23bh}$ mutants (n=96 embryos scored)

(J-L) Confocal images of *Tg(fli1a:nEGFP); Tg(-5.2lyve1b:DsRed)* *sec23a*^{uq23bh} embryos. Siblings display normal development of facial lymphatic vessels LFL, MFL, LAA, OLV, LL

LFL= lateral facial lymphatic; MFL= medial facial lymphatic; LAA = lateral branchial arches; OLV= otolithic lymphatic vessel; LL=lymphatic loop

(J,L) while *sec23a*^{uq22bh} have a significant reduction in LEC numbers in these vessels and a specific absence of the OLV at 5dpf (asterisk, K,L). Bars, 30μm

(M) Quantification of vISVs at 54hpf reveals no difference between sibling and *sec23a*^{uq23bh} embryos.

(N-Q) Confocal images of *Tg(fli1a:nEGFP); Tg(-5.2lyve1b:DsRed)* sibling (N,P; n=15) and *sec23a*^{uq22bh} (O,Q; n=20) intestinal gut vasculature at 3dpf and 5dpf showing *sec23a*^{uq22bh} mutants have relatively normal ongoing intestinal vascular development at 3dpf with mild delay at 5dpf. Bars, 30μm

(R,S) Quantification of the nuclei in the intestinal gut vasculature (within the white box) showed no difference in sibling (n=15) and *sec23a*^{uq22bh} (n=20) at 3dpf (R) however, at 5dpf (S) there was a mild reduction in *sec23a*^{uq22bh} (n=10) compared to sibling (n=10) suggesting late developmental delay after 3dpf.

*=P value<0.05, **=P value<0.01,***=P value<0.001.

Supplementary Figure 3

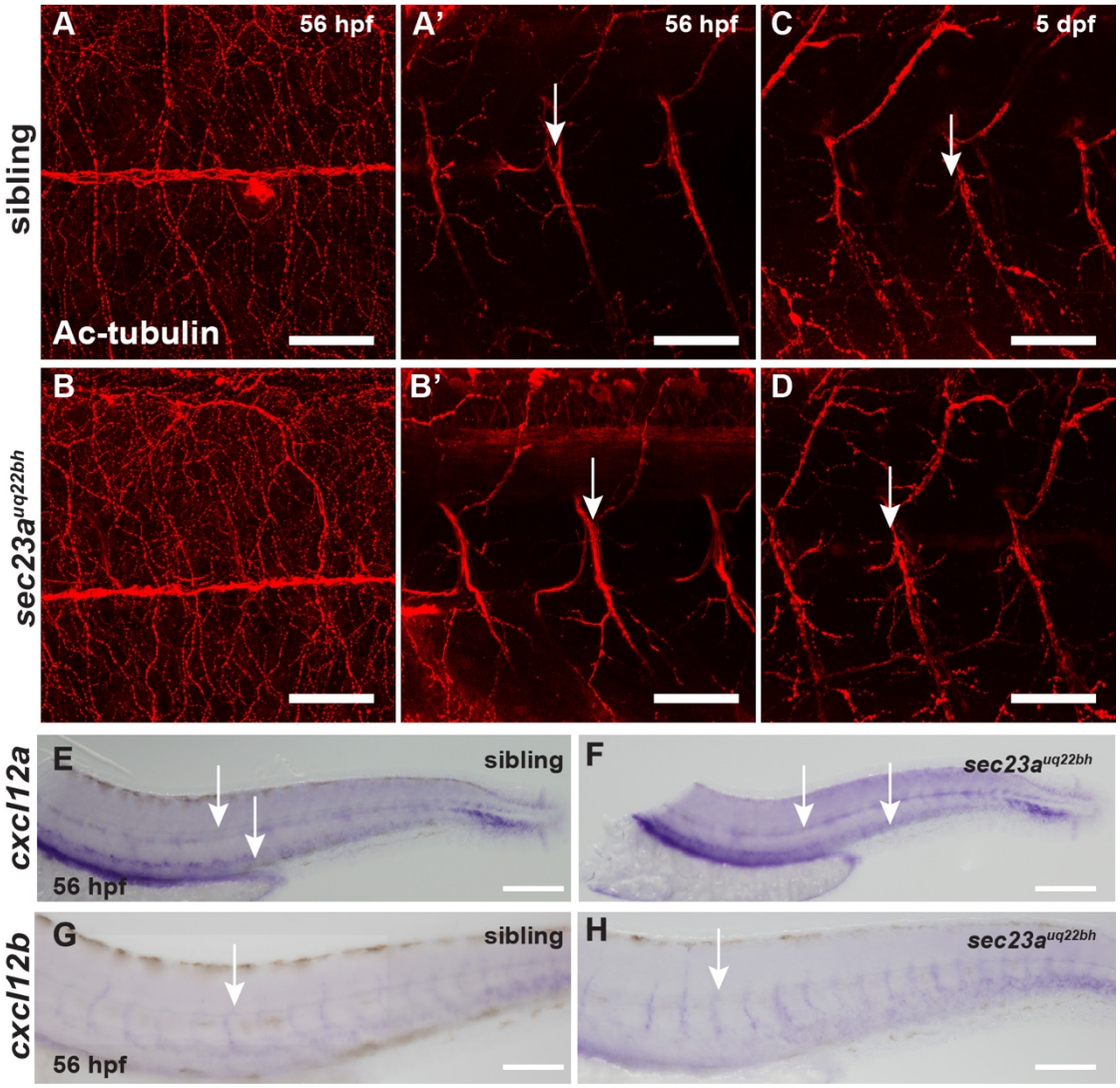

Fig. S3. *sec23a*^{uq22bh} mutants show no significant differences in motoneuron development and expression of chemokine ligands.

(A-D) Immunofluorescence assay showed normal expression of acetylated tubulin in motoneurons at 56hpf in siblings (A, A'; n=10), *sec23a*^{uq22bh} mutants (B, B'; n=10), 5dpf siblings (C; n=5) and *sec23a*^{uq22bh} mutants (D; n=5).

(E-F) Normal expression of *cxcl12a* was observed in the PCV in siblings (E; n=30) and *sec23a*^{uq22bh} mutants (F; n=10).

(G-H) *cxcl12b* expression was observed along arterial intersegmental vessels (aISVs) at 56hpf in siblings (G; n=30) and *sec23a*^{uq22bh} mutants (H; n=10).

Supplementary Figure 4

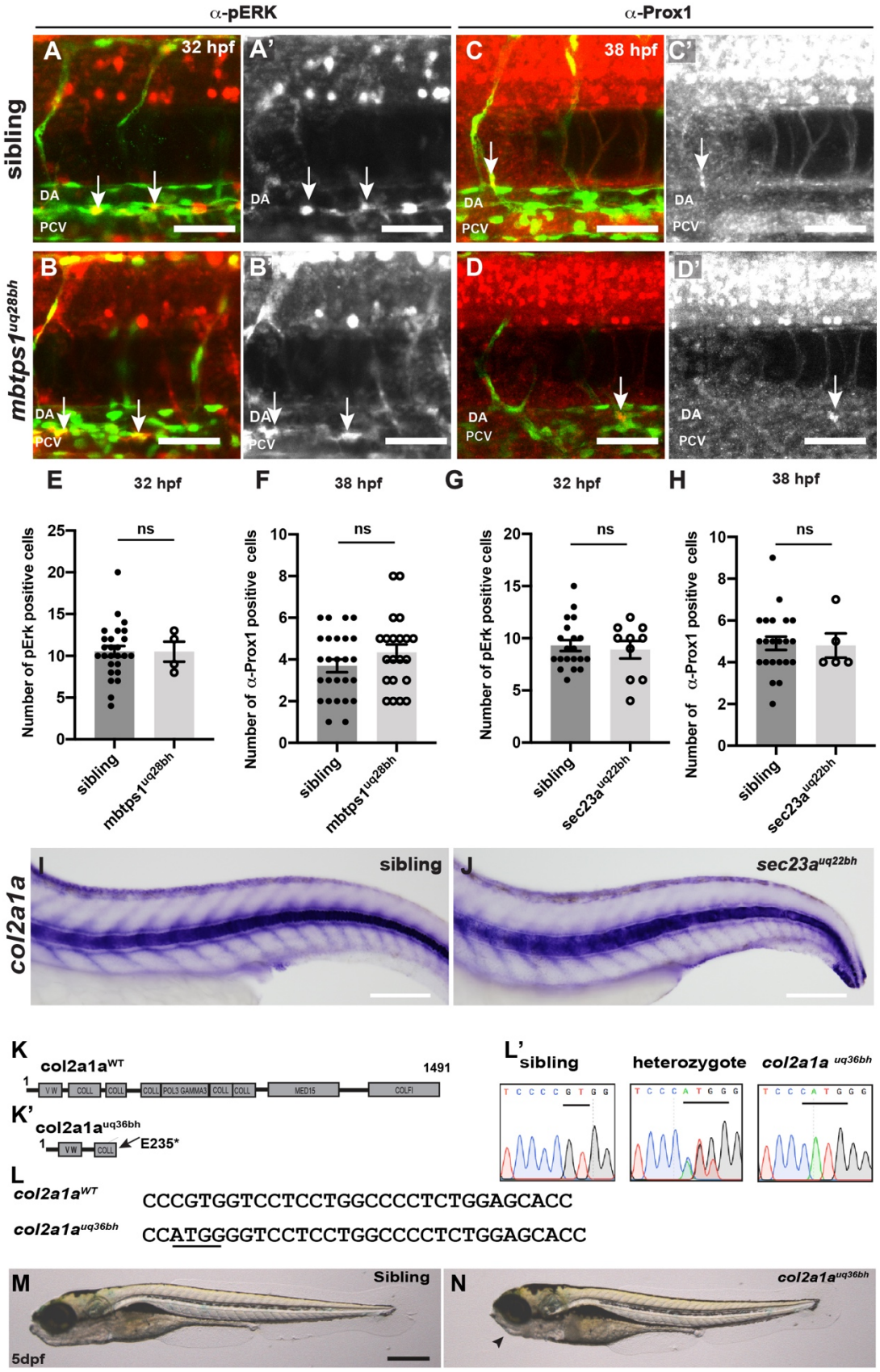

Fig. S4. *mbtps1*^{uq28bh} and *sec23a*^{uq22bh} mutants showed no significant differences in Prox1 and pErk expression in LECs

(A-B') Confocal images of *Tg(fli1a:nEGFP);* stained for eGFP (green) and p-Erk (red) in sibling (A; n=26) and *mbtps1*^{uq28bh} (B; n=4) (A', B' grayscale for pErk) at 32hpf showing the presence of pErk positive LECs (white arrows) on the dorsal side of the PCV.

(C-D') Confocal images of *Tg(fli1a:nEGFP);* stained for eGFP (green) and Prox1 (red) in sibling (C; n=26) and *mbtps1*^{uq28bh} (D; n=21) (C', D' grayscale for Prox1) at 38hpf showing the presence of Prox1 positive LECs (white arrows) on the dorsal side of the PCV.

(E,F) Quantification of pErk positive ECs (E) and Prox1-positive LECs (F) showed no significant difference between sibling and *mbtps1*^{uq28bh} embryos.

(G,H) No significant differences were observed on quantification of pErk positive LEC cells (G) and Prox1-positive LEC (H) between sibling and *sec23a*^{uq22bh} embryos.

(I,J) There was no difference in the expression of *col2a1a* in siblings (I; n=10) and *sec23a*^{uq22bh} mutants (J; n=10).

(K,L) CRISPR genome editing introduced a 3bp deletion/4bp (L,L') insertion and premature stop codon at amino acid 235 in *col2a1a*^{uq36bh} (K,K').

(M,N) Brightfield images showing short body axis in *col2a1a*^{uq36bh} when compared to siblings at 5dpf. Scalebars = 50μm

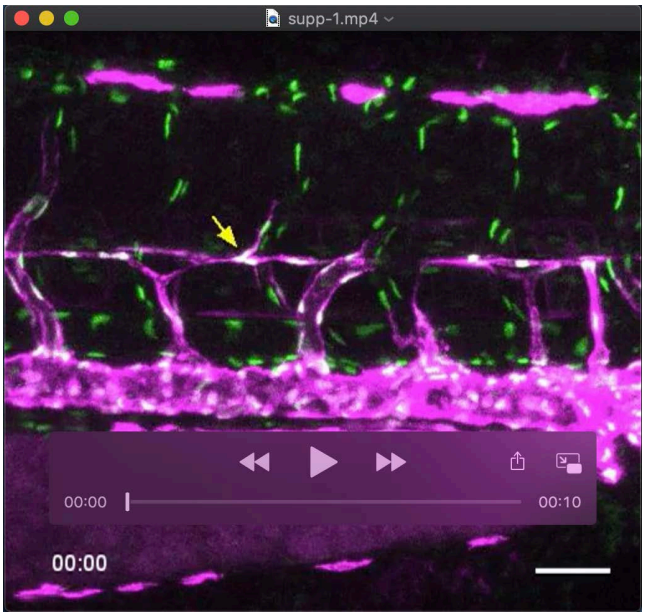

Movie 1. Time-lapse imaging of PLs in wildtype siblings from 65hpf to 78hpf. Arrow shows migration of PL dorsally

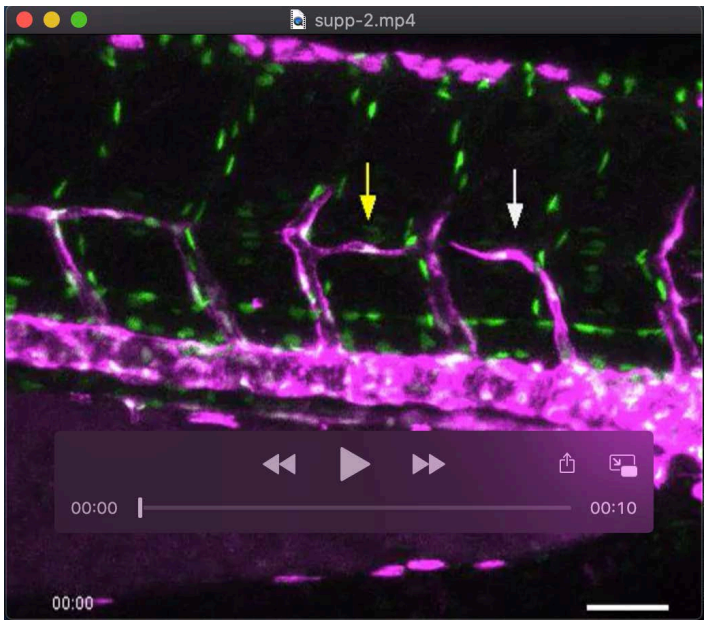

Movie 2. Time-lapse imaging of PLs in *sec23a*^{uq22bh} mutant from 65hpf to 78hpf. Yellow arrow shows a PL failing to migrate out of the HM. The white arrow shows a PL regressing.

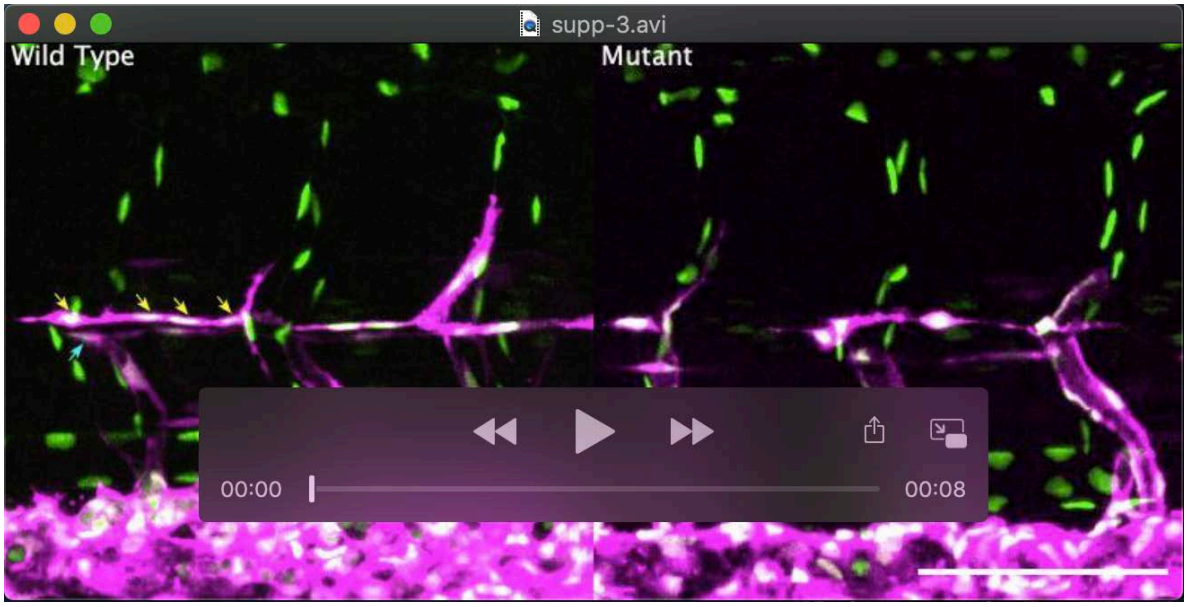

Movie 3. High speed spinning disk confocal time-lapse imaging of PLs in sibling (left panel) and *col2a1a*^{uq36bh} mutant (right panel) from 60-80hpf. Yellow arrows in the left panel highlight migration of LEC nuclei dorsally and blue arrows highlight migration ventrally. Representative of movies used to quantify phenotypes in Figures 4G & H.